Biomaterials and oxygen join forces to shape the immune response and boost SARS-CoV-2 vaccines

Thibault Colombani
Northeastern University https://orcid.org/0000-0003-3258-5093
Loek Eggermont
Northeastern University https://orcid.org/0000-0002-2151-7653
Zachary Rogers
Northeastern University
Lindsay McKay
Boston University School of Medicine
Laura Avena
Boston University School of Medicine
Rebecca Johnson
Boston University School of Medicine
Nadia Storm
Boston University School of Medicine
Anthony Griffiths
Boston University School of Medicine
Sidi Bencherif (s.bencherif@northeastern.edu)
Northeastern University https://orcid.org/0000-0002-7704-5608

Article

Keywords: Protective Antibodies, Protein Subunit Vaccines, Immune Stimulation, Immunological Co-adjuvant

Posted Date: November 11th, 2020

DOI: https://doi.org/10.21203/rs.3.rs-102055/v1

Abstract

Severe acute respiratory syndrome coronavirus 2 (SARS-CoV-2) has led to an unprecedented global health crisis, resulting in a critical need for effective vaccines that generate protective antibodies. Protein subunit vaccines represent a promising approach but often lack the immunogenicity required for strong immune stimulation. To overcome this challenge, we first demonstrate that advanced biomaterials boost effectiveness of SARS-CoV-2 protein subunit vaccines. Additionally, we report that oxygen is a powerful immunological co-adjuvant, a game-changer in the field for unlocking the full potential of vaccines. Mice immunized with oxygen-generating cryogel vaccines exhibited a robust and balanced Th1 and Th2 immune response, leading to sustained and high titer production of neutralizing antibodies against SARS-CoV-2. Our data indicate that this platform is a revolutionary technology with the potential to reinforce any vaccine.

Main

Severe acute respiratory syndrome coronavirus 2 (SARS-CoV-2) has caused a global pandemic with over 30 million cases and nearly 1 million deaths as of September 2020 with no indications of slowing down[1]. In response, several strategies are currently under rapid investigation, including treatments (e.g., antivirals, antibodies, anti-inflammatory, and immunomodulatory factors)[2–4], and prophylactic vaccines (e.g., nucleic acid-based, protein subunit-based, recombinant viral vector-based, inactive or attenuated viral-based, virus-like particles)[5–7]. Yet, only vaccines have the potential to confer global immunity. The stakes are high: The alternative is natural herd immunity, requiring several waves of infection over the next few years, a period characterized by high mortality, economic uncertainty, and a perturbed way of life[8]. There are several promising vaccine candidates in the clinic, but to date, it is unclear whether they will be approved or, more importantly, alter the course of the pandemic[7]. Therefore, there is a critical need to continue driving novel vaccination platforms into the clinic until SARS-CoV-2 is quelled, as well as to prepare for future pandemics.

Protein subunit vaccines have been approved to protect against infectious diseases with several currently commercially available[9], yet they lack the immunogenicity required to induce strong, long-lasting immunity[5,10]. Biomaterial-based delivery systems can address this challenge[11] by enhancing vaccine immunogenicity while reducing toxicity through controlled presentation and release of antigens and immunomodulatory factors (e.g., cytokines and adjuvants)[12]. Cryogels, polymeric biomaterials with a unique interconnected macroporous network, can be used as a platform to recruit, host, and program immune cells in situ. Previously, cryogels have been tested as cancer vaccines with promising results in preclinical melanoma and breast cancer models[13,14]. Therefore, we hypothesized that a cryogel-based SARS-CoV-2 vaccine, consisting of immunomodulatory factors and viral antigens, would provide an effective platform for dendritic cell (DC) activation while stimulating antibody-producing B cells in the draining lymph nodes (LNs). This strategy is expected to induce high numbers of binding and neutralizing antibodies, resulting in effective protection against SARS-CoV-2 infection.

One major challenge we anticipated when priming DCs within the subcutaneously injected cryogel is the lack of local vascularization. This environment induces low oxygen tension (hypoxia) due to an imbalance between oxygen supply and consumption (Fig. 1A). Our results indicated that hypoxic conditions of the subcutaneously injected cryogel suppress DC activation, which is consistent with previous reports[15,16]. Therefore, we engineered oxygen-generating cryogels (O_2-Cryogels) to mitigate hypoxia-driven immunosuppression[17]. In vivo, the number of hypoxic cells was decreased within subcutaneously injected O_2-Cryogels compared to standard cryogels (Fig. 1A). In vitro, O_2-Cryogels restored DC activation by CpG-ODN 1826, increasing the percent of cells positive for activation markers CD86 and CD317 to levels similar to DCs stimulated under normoxic conditions (Fig. 1B). Thus, we proposed that local oxygen supply within cryogel vaccines could potentiate SARS-CoV-2 protein subunit vaccines.

Results

SARS-CoV-2 vaccine fabrication and characterization

Hyaluronic acid-based cryogel vaccines were fabricated by cryogelation, as previously described (Fig. 1C, steps 1–3)[13,18,19]. This process results in an elastic biomaterial with a highly interconnected macroporous network, allowing immune cells to traffic in and out of the cryogel. To fabricate cryogel-based SARS-CoV-2 vaccines, we incorporated both the nucleocapsid protein (N), which encapsulates the virus RNA and the receptor-binding domain (RBD) of the spike protein (S) that is responsible for virus entry into cells. The cryogels also contained granulocyte macrophage colony-stimulating factor (GM-CSF), a molecule that stimulates and promotes recruitment of various immune cells, including DCs[18,20], and the adjuvant CpG-ODN 1826, a ligand for TLR9 (toll-like receptor 9) that recruits and activates DCs, specifically plasmacytoid DCs (pDCs)[21–23]. These cryogel-based vaccines were formulated to induce a robust humoral immune response[23,24]. To enhance vaccine immunogenicity, oxygen was considered as an immunological co-adjuvant that would eliminate local hypoxia at the site of vaccine administration[25]. Thus, oxygen-producing calcium peroxide (CaO_2) particles and acrylate-PEG-catalase (APC) were incorporated within the cryogel vaccine formulations before freezing, as previously described[17]. The resulting O_2-Cryogel vaccine was designed to generate oxygen upon the reaction of CaO_2 with water and to eliminate hydrogen peroxide byproducts through a catalase-mediated breakdown.

Following subcutaneous immunization (Fig. 1C), we hypothesized that cryogel-based protein subunit vaccines would induce DC-mediated humoral immunity (Fig. 1D)[18]. Sustained release of immunomodulatory factors (GM-CSF and CpG-ODN 1826) promotes DC infiltration into the macroporous network of cryogels, wherein DCs would uptake protein antigens (N and RBD proteins) and simultaneously become activated by CpG-ODN 1826 and the increased local oxygen tension. Activated, antigen-loaded DCs would migrate to draining LNs to initiate the activation of antigen-specific T cells and B cells. Furthermore, protein antigens and adjuvants released from the cryogel would also drain to the

draining LNs, directly enhancing B cell and DC activation. A subset of activated B cells would differentiate into plasma cells with the primary role of producing large quantities of SARS-CoV-2-binding antibodies. A fraction of these antibodies would be neutralizing antibodies and exert their inhibitory activity by abrogating binding of the virus RBD to the human receptor angiotensin-converting enzyme 2 (ACE2).

The encapsulation of RBD and N proteins within O_2-Cryogel$_{VAX}$ polymer walls was characterized by confocal microscopy and release from the cryogel by ELISA (Fig. S1A-B). Both proteins were effectively entrapped and colocalized within the polymer network. Both Cryogel$_{VAX}$ and O_2-Cryogel$_{VAX}$ exhibited an initial burst release of their payload, followed by a sustained release of the immunomodulatory factors GM-CSF and CpG-ODN 1826 and the antigen RBD (Fig. S1B). Notably, there were no differences among the encapsulation (Fig. S1C) and release profiles of CpG-ODN 1826, GM-CSF, and RBD for the two types of cryogels. Importantly, no significant amounts of Ca^{2+} or H_2O_2 are released from O_2-Cryogels (Fig. S1D-E), further indicating that they are non-toxic and can safely be used in vivo, as also demonstrated previously[17]. These results suggested that cryogels and O_2-Cryogels are suitable platforms for controlled vaccine delivery.

O_2-Cryogel$_{VAX}$ and Cryogel$_{VAX}$ induce high antibody titers with strong neutralizing activity

To test the vaccines, eight-week-old female BALB/c mice were immunized by subcutaneous injection of two O_2-Cryogel$_{VAX}$ or Cryogel$_{VAX}$ (one on each flank) at day 0 (prime) and day 21 (boost) (Fig. 2A). Control groups were injected with either PBS (sham–negative control), cryogel-free vaccine (Bolus$_{VAX}$), or Freund's-based vaccine (Freund$_{VAX}$–positive control) (Table 1). Blood serum analysis revealed that, although low titers of immunoglobulin M (IgM) antibodies were found across all groups (Fig. S2A), Cryogel$_{VAX}$ and O_2-Cryogel$_{VAX}$ induced high titers of RBD-specific binding immunoglobulin G (IgG) antibodies after only 21 days (Fig. 2B and Fig. S2B). These titers increased substantially following boost immunization, peaking at 1.4×10^6 at day 42 for animals immunized with Cryogel$_{VAX}$ and 3.1×10^6 at day 56 for animals immunized with O_2-Cryogel$_{VAX}$, amounts two orders of magnitude greater than those in control groups. Interestingly, O_2-Cryogel$_{VAX}$ induced higher production of RBD-specific binding IgG antibodies than Cryogel$_{VAX}$ did, and these titers were sustained for nearly 2 months (study endpoint). Similarly, O_2-Cryogel$_{VAX}$ immunization resulted in high titers of N-specific binding IgG antibodies comparable to those induced by Freund$_{VAX}$, and 3- and 5-times higher than those generated by Cryogel$_{VAX}$ and Bolus$_{VAX,}$ respectively.

Table 1
SARS-CoV-2 vaccination groups and dosage

Group	Formulation
Sham	2 × 100 µL PBS
$Freund_{VAX}$	1 × 100 µL [(25 µg RBD + 25 µg N proteins + 1.5 µg GM-CSF – 1:1 ratio with complete Freund's adjuvant (CFA – Prime) or incomplete Freund's adjuvant (IFA – Boost)]
$Bolus_{VAX}$	2x [(10 µg RBD + 10 µg N proteins + 1.5 µg GM-CSF + 50 µg ODN1826) + 100 µL PBS]
$Cryogel_{VAX}$	2x [(10 µg RBD + 10 µg N proteins + 1.5 µg GM-CSF + 50 µg ODN1826) + 100 µL PBS]
O_2-$Cryogel_{VAX}$	2x [(10 µg RBD + 10 µg N proteins + 1.5 µg GM-CSF + 50 µg ODN1826 + 200 µg of APC + 200 µg CaO_2) + 100 µL PBS]

To detect neutralizing antibodies that target the viral spike (S) protein RBD and block its interaction with ACE2, we performed a SARS-CoV-2 surrogate virus neutralization test (sVNT) (Fig. 2C and Fig. S2C). In agreement with the high serological IgG titers, O_2-$Cryogel_{VAX}$ elicited the strongest neutralizing antibody response, with a reciprocal IC_{50} titer of nearly 20,000 at day 56, which is 3- and 100-fold higher than those from $Cryogel_{VAX}$ and control groups ($Bolus_{VAX}$ and $Freund_{VAX}$), respectively. Additionally, neutralizing antibodies induced within 3 weeks after only a single immunization with O_2-$Cryogel_{VAX}$ were comparable to those induced after 8 weeks in mice receiving prime and boost vaccinations with $Bolus_{VAX}$ or $Freund_{VAX}$ (Fig. 2C, upper). Importantly, 1.7% of O_2-$Cryogel_{VAX}$-induced anti-RBD IgG antibodies were neutralizing from day 21 onward (Fig. 3C, lower). We also assessed the neutralization potency of antibodies by plaque reduction neutralization test (PRNT) using VeroE6 cells infected with authentic SARS-CoV-2 (Fig. 2D)[26]. As expected, O_2-$Cryogel_{VAX}$ immunization led to high neutralizing titers, which intensified from day 21, reaching a reciprocal IC_{50} value of nearly 10,000 at day 56 (study endpoint). Collectively, these data demonstrated that the cryogel platform potentiates vaccine efficacy. Furthermore, additive oxygen as a co-adjuvant strongly boosted the humoral response, as shown by the production of antibodies with high neutralizing activity.

O_2-$Cryogel_{VAX}$ promotes local immune cell recruitment and B cell production in LNs

To understand how the vaccines work, we characterized the immune response following prime and prime-boost immunizations in mice. At day 21 and 56, draining LNs, spleens, and cryogels were explanted (Fig. 2A). In comparison to the injection sites of $Cryogel_{VAX}$, sites of both prime and boost O_2-$Cryogel_{VAX}$ injections were markedly enlarged, indicating increased inflammation and immune cell infiltration (Fig. 3A). Overall, unlike blank cryogels, large numbers of infiltrated immune cells were retrieved from

both types of cryogel vaccines (Fig. 3B and Fig. S3A, S3B). Most explanted cryogels exhibited low and comparable numbers of CD4 + and CD8 + T cells, whereas high numbers of CD11b-positive myeloid cells, but no DCs, were present (Fig. 3B). Furthermore, the total number of cells positive for the B cell marker CD19 was 2-fold higher in O_2-Cryogel$_{VAX}$ compared to those in blank cryogels (Fig. S3B). However, the exact identity of these cells is unclear, as they were also CD11b-positive and did not have other B cell markers such as MHCII (Fig. S3A). Additionally, only a small population of MHCII-positive CD11b + cells was observed. Interestingly, evidence for an ongoing adaptive immune response was found in a small number of cryogel vaccines. These cryogel vaccines contained a lower fraction of CD11b + myeloid cells but relatively greater proportions of T cells and MHCII + B cells (see the outliers in Fig. 3B and Fig. S3B). Compared to day 21, immune cell numbers in prime cryogel vaccines decreased at day 56, indicating that both types of cryogel vaccines do not generate chronic and potentially dangerous inflammatory responses. However, cell counts in boost O_2-Cryogel$_{VAX}$ were slightly, but significantly, increased compared to other cryogel vaccines at day 56.

Analysis of LNs in mice immunized with Cryogel$_{VAX}$ and O_2-Cryogel$_{VAX}$ confirmed that a robust immune response was induced. This resulted in at least a 4-fold greater increase in total immune cell numbers than that observed among mice receiving sham injections at both time points (Fig. 3C and Fig. S4A, S4B). In particular, the frequency of MHCII + B cells within LNs was greatly increased in mice immunized with both cryogel-based vaccines. Although the frequency of CD4 + T cells was reduced at day 21 in LNs from mice receiving cryogel vaccines (Fig. 3C), overall CD4 + and CD8 + T cell numbers increased after vaccination (Fig. S4B). These data showed that cryogel vaccines induce a strong B cell-mediated immune response in LNs and display restrained adaptive immune responses within the cryogels following initial priming.

O_2-Cryogel$_{VAX}$ induces balanced Th1/Th2-associated immune responses

Previous reports with experimental SARS-CoV vaccines[27–29] indicated that an unbalanced T helper 1 (Th1) and T helper type 2 (Th2) immune responses, especially when biased towards Th2, is associated with poor clinical outcomes in infected patients[30,31] due to vaccine-associated enhanced respiratory disease (VAERD). Therefore, we analyzed the balance between Th1 and Th2 immune responses. Production of antibody subclass IgG1 is indicative of Th2 responses, and IgG2a/b/c and IgG3 are indicative of Th1 responses[32]. In our study, vaccines across all groups elicited IgG2 and IgG1 subclass RBD-binding antibodies, indicating induction of both Th1 and Th2 immune responses (Fig. 4A). Both cryogel-based vaccines promoted the production of IgG2b. However, O_2-Cryogel$_{VAX}$ enhanced Th2-biased antibody production as high titers of IgG1 were found in immunized mice resulting in lower IgG2a/IgG1 and IgG2b/IgG1 ratios (Fig. 4B). Interestingly, O_2-Cryogel$_{VAX}$ was the only vaccine that induced IgG3 production, which is associated with Th1 responses (Fig. 4A–B).

Th1 and Th2 responses are also associated with different cytokine profiles: interferon γ (IFNγ), tumor necrosis factor α (TNFα), and interleukin-2 (IL-2) indicate Th1 responses; IL-4, IL-5, and IL-13 indicate Th2 responses. Thus, we quantified cytokines in serum at day 24 (Fig. 5C) and in explanted cryogels at day 56 (Fig. 4D). At day 24, all vaccines induced high concentrations of pro-inflammatory interleukin-6 (IL-6) and Th1 cytokines (IFNγ and TNFα) in mouse sera (Fig. 4C). Strikingly, concentrations of IFNγ and IL-6 in mice immunized with O_2-Cryogel$_{VAX}$ were 3- or 10-fold higher than their concentrations in mice immunized with Bolus$_{VAX}$ or Cryogel$_{VAX}$, respectively. Similar results were observed at day 56 (Fig. 4D). Higher concentrations of Th1 cytokines IFNγ, TNFα, and IL-2, as well as IL-6, were quantified in mice immunized with O_2-Cryogel$_{VAX}$, compared to those immunized with Cryogel$_{VAX}$. Furthermore, we noted low concentrations of the Th2 cytokine IL-13 in O_2-Cryogel$_{VAX}$. As expected, blank cryogels were associated with low or negligible amounts of these cytokines.

To more directly assess the Th1/Th2 balance, we investigated the cytokine profile of antigen-specific T cells generated with both cryogel vaccines. The intracellular production of cytokines by splenocytes from immunized mice was examined following stimulation with peptides derived from viral S or N proteins. Cells were isolated at day 21 after prime immunization. Splenocytes from O_2-Cryogel$_{VAX}$-immunized mice stimulated with N-derived peptides showed increased fractions of IL-5-producing CD4 + and CD8 + T cells and IL-13-producing CD4 + T cells (Fig. 4E and fig. S5). These results indicated the presence of N protein-specific Th2 cells. However, no differences were noted following stimulation with S-derived peptides, and the proportions of IFNγ–, IL-4–, or IL-17–producing T cells were also comparably low. Collectively, these data suggested that both types of cryogel vaccines elicited a balanced Th1/Th2 immune response, even though it was more prominent for O_2-Cryogel$_{VAX}$.

Discussion

Nearly every decade for the past 30 years, a novel coronavirus pandemic emerges, pushing the healthcare system to its limit[33]. Although the current outbreak had long been predicted, SARS-CoV-2 has created the most severe crisis in recent history[34,35]. The rapid development of an effective and safe vaccine against this virus is the most effective strategy to end this pandemic. Among them, protein subunit vaccines have been widely investigated against SARS-CoV-2 due to their performance and safety record, and such vaccines have already shown promising early results in phase 1/2 clinical trials[11]. Yet, subunit vaccines still have to overcome their poor immunogenicity[36]. In addition, an ideal antiviral vaccine should be versatile and rapid to design, enabling rapid response to the public health emergency. To overcome these challenges, our team leveraged a cryogel-based vaccine platform to strengthen protein subunit vaccines and induce a strong and sustained anti-SARS-CoV-2 immune response[18]. In addition, we showed that oxygen is a powerful immunological co-adjuvant that shapes and reinforces the immune response. This work demonstrated how robust and modular the cryogel-based vaccine technology is, which was successfully and quickly adapted from cancer to an infectious disease at breakneck speed (< 3 months).

We found that Cryogel$_{VAX}$ induces a balanced Th1/Th2 immune response while enhancing the efficacy of a conventional protein subunit vaccine by 100-fold (Bolus$_{VAX}$). This is most likely due to the ability of cryogels to control the release of immunomodulatory factors while activating high numbers of resident immune cells. Following prime-boost immunization, Cryogel$_{VAX}$ elicited a strong humoral immune response for nearly 2 months (study endpoint) and was associated with high levels of anti-RBD IgG antibodies and strong neutralizing activity to SARS-CoV-2. In addition, Cryogel$_{VAX}$ induced CD4 + and CD8 + T cell responses, specifically directed against the N protein. The unique macroporous architecture of Cryogel$_{VAX}$ and incorporation of a chemoattractant also promoted the recruitment of large numbers of resident leukocytes and CD19 + immune cells, leading to increased expansion of B cells in the LNs within 21 days. This supports our hypothesis that Cryogel$_{VAX}$ acts as a distant immune cell training platform, jump-starting, and reinforcing our prime–boost vaccination strategy.

Although promising, Cryogel$_{VAX}$ has been associated with a number of limitations, including a decrease in anti-SARS-CoV-2 IgG antibodies after 42 days and low concentrations of Th1 cytokines. In light of these findings, we explored the use of oxygen as an immunological co-adjuvant to potentiate Cryogel$_{VAX}$ efficacy. We demonstrated that supplemental oxygen not only promoted CD4 + and CD8 + T cell responses against SARS-CoV-2, but also induced the production of Th1-biased and pro-inflammatory cytokines. On top of this, O_2-Cryogel$_{VAX}$ remarkably boosted humoral immunity with increased concentrations of both binding and neutralizing IgG1 antibodies against the virus. This suggests the induction of strong Th1 and Th2-associated immune responses. Interestingly, O_2-Cryogel$_{VAX}$ promoted local recruitment of leukocytes, notably CD19 + cells, and enhancement of B cell expansion in the LNs. Altogether, this study clearly demonstrated that oxygen is a key vaccine component and plays an important role in shaping the immune response, ultimately unleashing the full potential of vaccines.

More research is needed to assess the duration of our vaccine-induced immune responses, especially in non-human primates and humans, as well as to more carefully dissect the immune mechanism by which both the humoral and cell-based immune responses are triggered[37,38]. Furthermore, examining immune cell populations at earlier time points, the synergistic interaction of N and RBD proteins during immune priming, in addition to the contribution of each of the immunomodulatory factors and their optimal release kinetics, may further shed light on the vaccine mode of action. Moreover, a deeper understanding of the spatiotemporal diffusion of oxygen could be leveraged to further boost vaccine efficacy. Finally, additional studies are required to evaluate the long-term protection by and safety of O_2-Cryogel$_{VAX}$, as well as their effectiveness in aged or obese animals.

In summary, our study unveils the magnitude of an advanced biomaterial-based technology to harness the power of protein subunit vaccines, leading to a rapid and protective anti-SARS-CoV-2 immune response. Additionally, we report the synergistic effect of vaccines engineered to provide oxygen as a powerful immunological co-adjuvant. Lastly, although our efforts focused on protein subunits, this platform is compatible with other strategies, such as live attenuated or inactivated pathogens and nucleic acid vaccines, and may boost the efficiency of existing vaccines or those under development. Because

vaccinologists believe the first generation of the vaccines currently in clinical trials might not be optimal, our study opens new possibilities to leverage the COVID-19 vaccines that are in clinical trials and develop improved versions.

Methods

Cryogel fabrication

Cryogels were fabricated as previously described by redox-induced free radical cryopolymerization of hyaluronic acid glycidyl methacrylate (HAGM – 4% wt/vol) at subzero temperature (-20 °C)[13,17,18]. Briefly, the polymer solution was precooled at 4 °C prior to adding tetramethylethylenediamine (TEMED – 0.42% wt/vol, Sigma-Aldrich) and ammonium persulfate (APS – 0.84% wt/vol, Sigma Aldrich). Then, the mixture was transferred into Teflon® molds (4 × 4 × 1 mm, cubiform with 2 square-shaped sides, 16 µL), placed in a freezer at -20 °C, and allowed to cryopolymerize for 16 h. Finally, the newly formed cryogels were thawed at room temperature (RT) to remove ice crystals and washed with Dulbecco's Phosphate Buffered Saline (DPBS, Gibco). For O_2-Cryogel fabrication, acrylate-PEG-catalase (APC – 1% wt/vol, Sigma-Aldrich) and calcium peroxide (CaO_2 – 1% wt/vol) were mixed with the cryogel polymer solution before the addition of TEMED and APS as previously reported[17].

SARS-CoV-2 vaccine fabrication

Protein subunit-based vaccines were fabricated by formulating (1) purified recombinant SARS-CoV-2 Spike (ΔTM) his-tagged protein (RBD, 10 YP_009724390.1 - Arg319-Phe541, Creative Biomart nCoVS-125V), (2) purified recombinant 2019-nCoV Nucleocapsid protein (N, YP_009724397.2, Creative Biomart N-127V), purified recombinant mouse granulocyte macrophage colony stimulating factor (mGM-CSF, GenScript), and synthetic immunostimulatory oligonucleotide containing unmethylated CpG dinucleotides (CpG ODN 1826, 5'-tccatgacgttcctgacgtt-3', VacciGrade, InvivoGen) in DPBS. For $Bolus_{VAX}$, 10 µg RBD, 10 µg N, 1.5 µg GM-CSF, and 50 µg CpG ODN 1826 were formulated in 100 µL of DPBS. For $Cryogel_{VAX}$ and O_2-$Cryogel_{VAX}$, 10 µg RBD, 10 µg N, 1.5 µg GM-CSF, and 50 µg CpG ODN 1826 (per gel) were incorporated within the polymer solution prior to cryogelation. After thawing, each cryogel-based vaccine was resuspended in 100 µL of DPBS. For $Freund_{VAX}$ (positive control), 25 µg RBD, 25 µg N, and 3 µg mGM-CSF were formulated in 50 µL DPBS and mixed at a 1:1 ratio with complete Freund's adjuvant (CFA - Prime) or incomplete Freund's adjuvant (IFA - Boost). Sham vaccine formulation containing only 100 µL DPBS was used as a negative control.

Mouse model and study design

Animal experiments were carried out in compliance with the National Institutes of Health (NIH) guidelines and approved by the Division of Laboratory Animal Medicine and Northeastern University Institutional Animal Care and Use Committee (protocol number 20-0629R). Vaccination studies were performed on 6-8-week-old female BALB/c (Charles River). $Freund_{VAX}$ was inoculated intraperitoneally (IP) (1 injection/mouse). Sham, $Bolus_{VAX}$, $Cryogel_{VAX,}$ and O_2-$Cryogel_{VAX}$ were injected subcutaneously (s.c.) in

both flanks (total of 2 injections/mouse). Boost injections were performed 21 days after priming at the same location. Blood samples were collected every seven days from day 14 onwards and three days post-boost (day 24). Cryogel-based vaccines, LNs, and spleens were harvested at day 21 (prime) and day 56 (prime + boost) and then dissociated as previously described[17,18]. Hypoxia studies were performed on 6-8-week-old female C57BL/6 mice (Charles River). Cryogels and O_2-Cryogels were suspended in 100 µL DPBS and injected s.c. into mouse flanks. After 23 h or 71 h, mice were injected IP with 200 µL of hypoxyprobe in DPBS (dosage: 60 mg/kg, hypoxyprobe), and 1 h after administration, the Cryogels and O_2-Cryogels were harvested, dissociated, and stained with FITC-MAb1 following manufacturer's recommendation. The number of hypoxic cells was then analyzed via flow cytometry using an Attune NxT flow cytometer (ThermoFisher).

BMDC generation for DC activation studies

Dendritic cells (DC) activation studies were performed using bone marrow-derived dendritic cells (BMDCs) generated from 6-8-week-old female C57BL/6 mice (Charles River) as previously described[18]. Briefly, femurs of mice were explanted, disinfected in 70% ethanol for 5 min, washed in DPBS, and then bone ends were removed, and the marrow flushed with DPBS (2 mL, 27G needle). Next, cells were mechanically dissociated by pipetting, centrifuged (5 min, 300 g), and resuspended (10^6 cells/mL) in Roswell Park Memorial Institute Medium (RPMI 1640, Gibco) supplemented with 10% heat-inactivated fetal bovine serum (FBS, Sigma Aldrich), 100 U/mL penicillin (Gibco), 100 µg/mL streptomycin (Gibco), 2×10^{-3} M L-glutamine (Gibco), and 50×10^{-6} M 2-mercaptoethanol (Gibco). At day 0, bone marrow–derived cells were seeded in non-treated p6 well plates (2×10^6 cells per well) in 5 mL of complete RPMI medium supplemented with 20 ng/mL mGM-CSF. At day 3, another 5 mL of RPMI medium containing 20 ng/mL mGM-CSF was added to each well. At days 6 and 8, half of the media was sampled from each well, centrifuged, and the cell pellet was resuspended in 5 mL of fresh RPMI media supplemented with only 10 ng/mL mGM-CSF before re-plating. BMDCs were collected at day 10 (non-adherent cells) and used to evaluate DC activation in normoxia or hypoxia.

In vitro DC activation assay

BMDCs were incubated in complete RPMI medium containing 10 ng/mL mGM-CSF at 37 °C in either humidified 5% CO_2/95% air (normoxia) or 5% CO_2/1% O_2/94% N_2 (hypoxia) incubator (Napco CO_2 1000 hypoxic incubator, ThermoFisher) for 24 h. One cryogel or O_2-Cryogel was added to each well prior to starting the incubation. For BMDC activation, the medium was completed with 5 µg/mL CpG ODN 1826. The negative control consisted of BMDCs cultured in complete RPMI medium containing 10 ng/mL mGM-CSF. DC stimulation and maturation was evaluated by flow cytometry using the following fluorescent antibodies (BioLegend): APC-conjugated anti-mouse CD11c (clone N418), PE-conjugated anti-mouse CD86 (Clone GL1), and PerCP/Cyanine5.5-conjugated anti-mouse CD317 (clone 927).

Imaging of encapsulated N and RBD proteins within the cryogel network

RBD or N protein was dissolved in sodium bicarbonate buffer (pH 8.5) at 0.5 mg/mL and reacted with Alexa Fluor 488-NHS ester or Alexa Fluor 647 NHS ester (Click Chemistry Tools), respectively, for 2 h at 4 °C. Fluorochrome-modified proteins were purified via spin filtration over 10 kDa Amicon Spin Filters (Sigma Aldrich) and washed 5 times with DPBS. Concentration of purified proteins was determined by UV-Vis absorbance measurements at 280 nm, after correcting for fluorophore absorbance, using the Nanodrop One (ThermoFisher). O_2-Cryogels containing the fluorescently labeled RBD and N proteins were fabricated as described above. After thawing, cryogels were washed four times with 1 mL of DPBS and imaged by confocal microscopy (Zeiss 800).

Release of immunomodulatory factors and antigens from cryogels

To determine the in vitro release kinetics of GM-CSF, CpG-ODN, and RBD protein from $Cryogel_{VAX}$ and O_2-$Cryogel_{VAX}$, gels were briefly washed in 70% ethanol followed by 2 DPBS washes. Each washed gel was incubated in sterile DPBS with 2% BSA in a microcentrifuge tube under orbital shaking at RT. The entire supernatant was removed periodically and replaced with the same amount of fresh buffer. GM-CSF, CpG-ODN, and RBD protein released in the supernatant were detected by either ELISA (GM-CSF: BioLegend ELISA MAX™ Deluxe, RBD: Elabscience SARS-CoV-2 Spike Protein S1 RBD ELISA Kit) or iQuant™ ssDNA quantification assay (GeneCopoeia). The N protein release kinetics was not determined due to the instability of the protein at high concentration, buffer, and study duration.

Antibody titration by enzyme-linked immunosorbent assay (ELISA)

Anti-RBD IgG and IgM antibody titers were determined using a SARS-CoV-2 Spike S1-RBD IgG&IgM ELISA detection kit (Genscript). Anti-N IgG and IgM antibody titers were determined using a SARS-CoV-2 Nucleocapsid Protein IgG ELISA Kit (Lifeome). Both kits were optimized by replacing the HRP-conjugated IgG or IgM anti-human antibody with an HRP-conjugated IgG (H + L) goat anti-mouse antibody (FisherScientific) or an HRP-conjugated IgM (Heavy chain) goat anti-mouse antibody (FisherScientific), respectively. Immunoglobulin isotyping was evaluated using Ig Isotyping Mouse Uncoated ELISA Kit (ThermoFisher) following the manufacturer's recommendation by measuring absorbance at 450 nm on a plate reader (Synergy HT). All ELISAs were performed on mouse sera that were heat-inactivated (30 min at 56 °C). Endpoint titers were determined as the maximum dilution that emitted an optical density exceeding 4 times the background (sera of mice vaccinated with Sham vaccine).

SARS-CoV-2 surrogate virus neutralization test (sVNT)

The detection of neutralizing antibodies against SARS-CoV-2 that block the interaction between RBD and the human ACE2 (hACE2) cell surface receptor was determined using an sVNT according to the manufacturer's protocol (Genscript). Briefly, heat-inactivated mouse sera were pre-incubated with HRP-RBD (30 min at 37 °C) to allow the specific binding of neutralizing antibodies. Then, the mixture was transferred into a plate coated with hACE2 and incubated for 15 min at 37 °C. The unbound HRP-RBD, as

well as HRP-RBD bound to non-neutralizing antibody, will interact with the hACE2, while neutralizing antibody–HRP-RBD complexes will remain in suspension and will be removed during washing. TMB substrate was used to detect the non-neutralized HRP-RBD. Therefore, the absorbance was inversely proportional to the titer of anti-SARS-CoV-2 neutralizing antibodies. For this experiment, 10-fold dilutions of mouse sera (10^{-1} to 10^{-8}) were used.

Cytokine quantification

Cytokine levels in mouse sera and cryogels were quantified using LEGENDplex™ mouse Th cytokine panel (BioLegend) according to the manufacturer's recommendations. Mouse sera were collected at day 24 (3-days post-boost) and diluted 10 and 100 times. $Cryogel_{VAX}$, O_2-$Cryogel_{VAX,}$ and (blank) cryogels were explanted at day 56, homogenized through a 70 µm cell strainer (FisherScientific), resuspended in 1 mL DPBS, and then centrifuged 5 min at 300 g. The supernatant was collected and diluted 2, 5, and 10 times. The cytokine panel included: IL-2, 4, 5, 6, 9, 10, 13, 17A, 17F, 22, IFNγ and TNFα.

Authentic SARS-CoV-2 plaque reduction neutralization test (PRNT)

Heat inactivated mouse serum samples were serially diluted in DPBS using two-fold dilutions starting at 1:50. Dilutions were prepared in duplicate for each sample and plated in duplicate. Each dilution was incubated in a 5% CO_2 incubator at 37 °C for 1 h with 1000 plaque-forming units/mL (PFU/mL) of SARS-CoV-2 (isolate USA-WA1/2020, BEI). Controls included (1) Dulbecco's Modified Eagle Medium (DMEM, Gibco) containing 2% fetal bovine serum (FBS, Gibco) and 100X antibiotic-antimycotic (Gibco) to a final concentration of 1X as a negative control; and (2) 1000 PFU/mL SARS-CoV-2 incubated with DPBS as a positive control. Each dilution or control (200 µL) was added to two confluent monolayers of NR-596 Vero E6 cells (ATCC) and incubated in a 5% CO_2 incubator at 37 °C for 1 h. A gentle rocking was performed every 15 min to prevent monolayer drying. Cells were then overlaid with a 1:1 solution of 2.5% Avicel® RC-591 microcrystalline cellulose and carboxymethylcellulose sodium (DuPont Nutrition & Biosciences) and 2x Modified Eagle Medium (MEM - Temin's modification, Gibco) supplemented with 100X antibiotic-antimycotic (Gibco) and 100X GlutaMAX (Gibco) both to a final concentration of 2X, and 10% FBS (Gibco). The plates were then incubated in a 5% CO_2 incubator at 37 °C for 2 days. The monolayers were fixed with 10% neutral buffered formalin for at least 6 h (NBF, Sigma-Aldrich) and stained with 0.2% aqueous Gentian Violet (RICCA Chemicals) in 10% NBF for 30 min, followed by rinsing and plaque counting. The half maximal inhibitory concentrations (IC_{50}) were calculated using GraphPad Prism 8 as previously described[26].

Immune cell characterization in cryogels and LNs

At day 21 and 56, cryogels and LNs were explanted, homogenized over a cell strainer, and single cell suspensions were washed with DPBS. Next, cells were stained with Fixable Viability Dye eFluor 506 (eBioscience, 1:1000 dilution in DPBS) for 30 min at 4 °C. The cells were washed once with DPBS and washed twice with PBA (PBS + 1%BSA) before staining of cell surface antigens by overnight incubation

of fluorochrome-conjugated antibodies (I-A/I-E-FITC (Clone: M5/114.15.2), CD138-PE (Clone 281-2), CD4-PerCP-Cy5.5 (Clone GK1.5), CD45.2-PE-Cy7 (Clone 104), CD11c-APC (Clone N418), CD8-AF700 (Clone 53 – 6.7), CD19-APC-Cy7 (Clone 6D5), CD11b-BV421 (Clone: M1/70), CD3-BV605 (Clone 145-2C11), Biolegend) in PBA at 4 °C. Cells were washed 3 times with PBA, fixed through incubation in 4% PFA in DPBS for 15 min at 4 °C, and washed 3 times with PBA. Flow cytometry measurements were done using the Attune NxT flow cytometer (ThermoFisher).

Splenocyte activation and intracellular cytokine staining

Splenocytes were incubated with 1) 20 ng/mL PMA (Sigma Aldrich) and 1 ug/mL ionomycin (Cell Signaling Technology) (Cell. 2) S protein-derived peptides (GenScript) 3) N protein-derived peptides (GenScript), or 4) control (no stimulation) in presence of 1X Brefeldin A and 1X Monensin (Biolegend) for 6 h at 37 °C. After this, the cells were washed with DPBS and incubated for 30 min with Fixable Viability Dye eFluor 780 (eBioscience) in DPBS (1:1000 dilution) at 4 °C. After this, cells were washed once with DPBS and washed twice with PBA before staining of cell surface antigens by overnight incubation of fluorochrome-conjugated antibodies (CD3-FITC (Clone 145-2C11), CD4-PerCP-Cy5.5 (Clone GK1.5), CD8-AF700 (Clone 53 – 6.7), CD44-BV605 (Clone IM7), Biolegend) in PBA at 4 °C. Cells were washed 3 times with PBA, after which they were fixed and permeabilized using the Cyto-Fast Fix/Perm Buffer Set (Biolegend) according to the manufacturer's protocol. Intracellular staining was done by incubation of cells with fluorochrome-conjugated antibodies (IL-13-PE (Clone: W17010B), IL-4-PE-Cy7 (Clone: 11B11), IL-17-APC (Clone: TC11-18H10.1), IL-5-BV421 (Clone: TRFK5), IFNγ-BV510 (Clone XMG1.2), Biolegend) in permeabilization buffer for 30 min at 4 °C. Cells were washed 3 times with permeabilization buffer, resuspended in PBA, and measured using the Attune NxT flow cytometer (ThermoFisher).

Statistical analysis

Flow cytometry data were analyzed using FlowJo software. Gating was done as depicted in Fig. S3A and S4A. Statistical analysis was performed using GraphPad Prism 5 software. Statistical significances were calculated with one-way ANOVA and Bonferroni post-tests to evaluate differences between time points (lines with dark stars indicate statistical differences) or two-way ANOVA and Bonferroni post-tests to evaluate the difference between different conditions/treatments (colored stars indicate statistical differences). P values of 0.05 or less were considered significant. Graphs show the mean ± SEM of calculated values.

Reporting summary

Further information on research design is available in the Nature Research Reporting Summary linked to this paper.

Data Availability

All data are available in the manuscript or the supplementary materials.

Declarations

Competing interests

The authors declare no conflicts of interest.

Author contributions

T.C., L.J.E, and S.A.B. conceived and designed the experiments. T.C., L.J.E., and Z.J.R. performed the experiments. T.C., L.J.E., Z.J.R., and S.A.B. analyzed the data and wrote the manuscript. T.C., L.J.E., Z.J.R., and S.A.B. conceived the figures. PRNT assay (Fig. 3D) was designed by L.G.A.M., performed by L.G.A.M., L.E.A., R.I.J., and N.S., and analyzed by T.C., R.I.J., and N.S. All authors discussed the results, commented on and proofread the manuscript. The principal investigator is S.A.B.

Acknowledgments

Authors thank Nancy R. Gough (BioSerendipity) for critical evaluation and editing assistance. Authors thank Richard Huffman and Nikolai Slavov for providing PMA and ionomycin. S.A.B. acknowledges support from Northeastern University (COVID-19 crisis award and GapFund360 award), NSF CAREER award (DMR 1847843), and the National Plan for Science, Technology, and Innovation (MAARIFAH), King Abdulaziz City for Science and Technology, the Kingdom of Saudi Arabia, award (15-MED5025-03).

References

1. Dong, E., Du, H. & Gardner, L. An interactive web-based dashboard to track COVID-19 in real time. *Lancet Infect. Dis.* **20**, 533–534 (2020).
2. Vijayvargiya, P. *et al.* Treatment Considerations for COVID-19. *Mayo Clin. Proc.* **95**, 1454–1466 (2020).
3. Sanders, J. M., Monogue, M. L., Jodlowski, T. Z. & Cutrell, J. B. Pharmacologic Treatments for Coronavirus Disease 2019 (COVID-19). *JAMA* **323**, 1824–1836 (2020).
4. Wiersinga, W. J., Rhodes, A., Cheng, A. C., Peacock, S. J. & Prescott, H. C. Pathophysiology, Transmission, Diagnosis, and Treatment of Coronavirus Disease 2019 (COVID-19). *JAMA* **324**, 782 (2020).
5. Jeyanathan, M. *et al.* Immunological considerations for COVID-19 vaccine strategies. *Nat. Rev. Immunol.* **20**, 615–632 (2020).
6. Koirala, A., Joo, Y. J., Khatami, A., Chiu, C. & Britton, P. N. Vaccines for COVID-19: The current state of play. *Paediatr. Respir. Rev.* **35**, 43–49 (2020).

7. Chen, W.-H., Strych, U., Hotez, P. J. & Bottazzi, M. E. The SARS-CoV-2 Vaccine Pipeline: an Overview. *Curr. Trop. Med. Reports* **7**, 61–64 (2020).
8. Graham, B. S. Rapid COVID-19 vaccine development. *Science* **368**, 945–946 (2020).
9. Moyle, P. M. & Toth, I. Modern Subunit Vaccines: Development, Components, and Research Opportunities. *ChemMedChem* **8**, 360–376 (2013).
10. Tsoras, A. N., Wong, K. M., Paravastu, A. K. & Champion, J. A. Rational Design of Antigen Incorporation Into Subunit Vaccine Biomaterials Can Enhance Antigen-Specific Immune Responses. *Front. Immunol.* **11**, 1547 (2020).
11. Keech, C. *et al.* Phase 1–2 Trial of a SARS-CoV-2 Recombinant Spike Protein Nanoparticle Vaccine. *N. Engl. J. Med.* (2020). doi:10.1056/NEJMoa2026920
12. Li, J. & Mooney, D. J. Designing hydrogels for controlled drug delivery. *Nat. Rev. Mater.* **1**, 16071 (2016).
13. Bencherif, S. A. *et al.* Injectable preformed scaffolds with shape-memory properties. *Proc. Natl. Acad. Sci. U. S. A.* **109**, 19590–19595 (2012).
14. Shih, T. Y. *et al.* Injectable, Tough Alginate Cryogels as Cancer Vaccines. *Adv. Healthc. Mater.* **7**, e1701469 (2018).
15. Paardekooper, L. M., Vos, W. & van den Bogaart, G. Oxygen in the tumor microenvironment: effects on dendritic cell function. *Oncotarget* **10**, 883–896 (2019).
16. Giovanelli, P., Sandoval, T. A. & Cubillos-Ruiz, J. R. Dendritic Cell Metabolism and Function in Tumors. *Trends Immunol.* **40**, 699–718 (2019).
17. Colombani, T. *et al.* Oxygen-generating cryogels restore T cell-mediated cytotoxicity in hypoxic tumors. *bioRxiv* 2020.10.08.329805 (2020). doi:10.1101/2020.10.08.329805
18. Bencherif, S. A. *et al.* Injectable cryogel-based whole-cell cancer vaccines. *Nat. Commun.* **6**, 7556 (2015).
19. Eggermont, L. J., Rogers, Z. J., Colombani, T., Memic, A. & Bencherif, S. A. Injectable Cryogels for Biomedical Applications. *Trends in Biotechnology* **38**, 418–431 (2020).
20. Ushach, I. & Zlotnik, A. Biological role of granulocyte macrophage colony-stimulating factor (GM-CSF) and macrophage colony-stimulating factor (M-CSF) on cells of the myeloid lineage. *J. Leukoc. Biol.* **100**, 481–489 (2016).
21. Haining, W. N. *et al.* CpG oligodeoxynucleotides alter lymphocyte and dendritic cell trafficking in humans. *Clin. Cancer Res.* **14**, 5626–5634 (2008).
22. Ali, O. A., Emerich, D., Dranoff, G. & Mooney, D. J. In situ regulation of DC subsets and T cells mediates tumor regression in mice. *Sci. Transl. Med.* **1**, 8ra19-8ra19 (2009).
23. Vollmer, J. *et al.* Characterization of three CpG oligodeoxynucleotide classes with distinct immunostimulatory activities. *Eur. J. Immunol.* **34**, 251–262 (2004).
24. Zhao, W., Zhao, G. & Wang, B. Revisiting GM-CSF as an adjuvant for therapeutic vaccines. *Cell. Mol. Immunol.* **15**, 187–189 (2018).

25. Hatfield, S. M. *et al.* Immunological mechanisms of the antitumor effects of supplemental oxygenation. *Sci. Transl. Med.* **7**, 277ra30 (2015).
26. Honko, A. N. Rapid quantification and neutralization assays for novel coronavirus SARS-CoV-2 using Avicel R RC-591 semi-solid overlay. (2020). doi:10.20944/preprints202005.0264.v1
27. Deming, D. *et al.* Vaccine efficacy in senescent mice challenged with recombinant SARS-CoV bearing epidemic and zoonotic spike variants. *PLoS Med.* **3**, 2359–2375 (2006).
28. Czub, M., Weingartl, H., Czub, S., He, R. & Cao, J. Evaluation of modified vaccinia virus Ankara based recombinant SARS vaccine in ferrets. *Vaccine* **23**, 2273–9 (2005).
29. Bolles, M. *et al.* A Double-Inactivated Severe Acute Respiratory Syndrome Coronavirus Vaccine Provides Incomplete Protection in Mice and Induces Increased Eosinophilic Proinflammatory Pulmonary Response upon Challenge. *J. Virol.* **85**, 12201–12215 (2011).
30. Zhang, Y., Li, B. & Ning, B. The Comparative Immunological Characteristics of SARS-CoV, MERS-CoV, and SARS-CoV-2 Coronavirus Infections. *Front. Immunol.* **11**, 2033 (2020).
31. Li, C. K. *et al.* T Cell Responses to Whole SARS Coronavirus in Humans. *J. Immunol.* **181**, 5490–5500 (2008).
32. Lin, L., Gerth, A. J. & Peng, S. L. CpG DNA redirects class-switching towards 'Th1-like' Ig isotype production via TLR9 and MyD88. *Eur. J. Immunol.* **34**, 1483–1487 (2004).
33. Shin, M. D. *et al.* COVID-19 vaccine development and a potential nanomaterial path forward. *Nat. Nanotechnol.* **15**, 646–655 (2020).
34. Graham, B. S. & Sullivan, N. J. Emerging viral diseases from a vaccinology perspective: preparing for the next pandemic. *Nat. Immunol.* **19**, 20–28 (2018).
35. Cheng, V. C. C., Lau, S. K. P., Woo, P. C. Y. & Yuen, K. Y. Severe Acute Respiratory Syndrome Coronavirus as an Agent of Emerging and Reemerging Infection. *Clin. Microbiol. Rev.* **20**, 660–694 (2007).
36. Wang, N., Shang, J., Jiang, S. & Du, L. Subunit Vaccines Against Emerging Pathogenic Human Coronaviruses. *Front. Microbiol.* **11**, 298 (2020).
37. Reddy, S. T., Swartz, M. A. & Hubbell, J. A. Targeting dendritic cells with biomaterials: developing the next generation of vaccines. *Trends Immunol.* **27**, 573–579 (2006).
38. Takayama, K. In Vitro and Animal Models for SARS-CoV-2 research. *Trends Pharmacol. Sci.* **41**, 513–517 (2020).

Figures

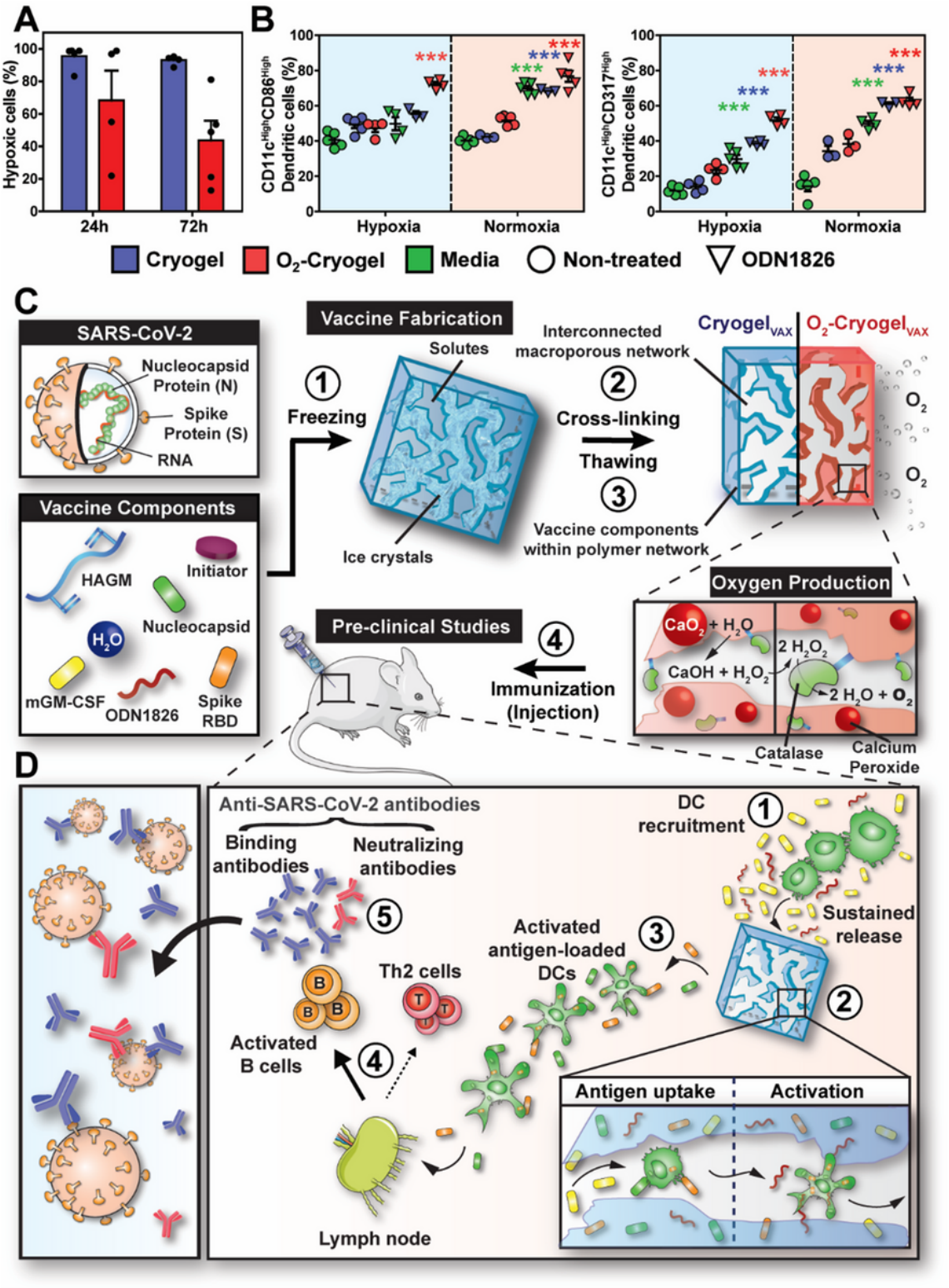

Figure 1

Cryogel-based vaccines reinforce DC-mediated immune responses. (A) Quantification of cellular hypoxia in cells recruited within Cryogels and O2-Cryogels 24 h and 72 h post-subcutaneous injection in mice. (B) Quantitative flow cytometric measurements of CD86High and CD317High dendritic cells (CD11cHigh) in Cryogels or O2-Cryogels in presence or absence of CpG-ODN 1826 in hypoxia and normoxia for 24 h (right panel). Values represent the mean ± standard error of the mean (SEM, n=5 per group). ***P < 0.001. (C)

Overview of the process for fabrication and evaluation of cubiform cryogel and O2-Cryogel vaccines. Step 1 involves freezing vaccine components, enabling crosslinking of solutes around ice crystals (step 2). Thawing results in an interconnected macroporous network with vaccine components encapsulated within the polymer network (step 3). Addition of calcium peroxide and catalase to the vaccine components before cryogelation produces O2-CryogelVAX capable of sustained production of oxygen. In step 4, cryogels are subcutaneously injected into mice for preclinical vaccine studies. (D) Illustration describing a model for DC-mediated cryogel-induced immunity. HAGM: hyaluronic acid glycidyl methacrylate; initiator: ammonium persulfate and tetramethylethylenediamine.

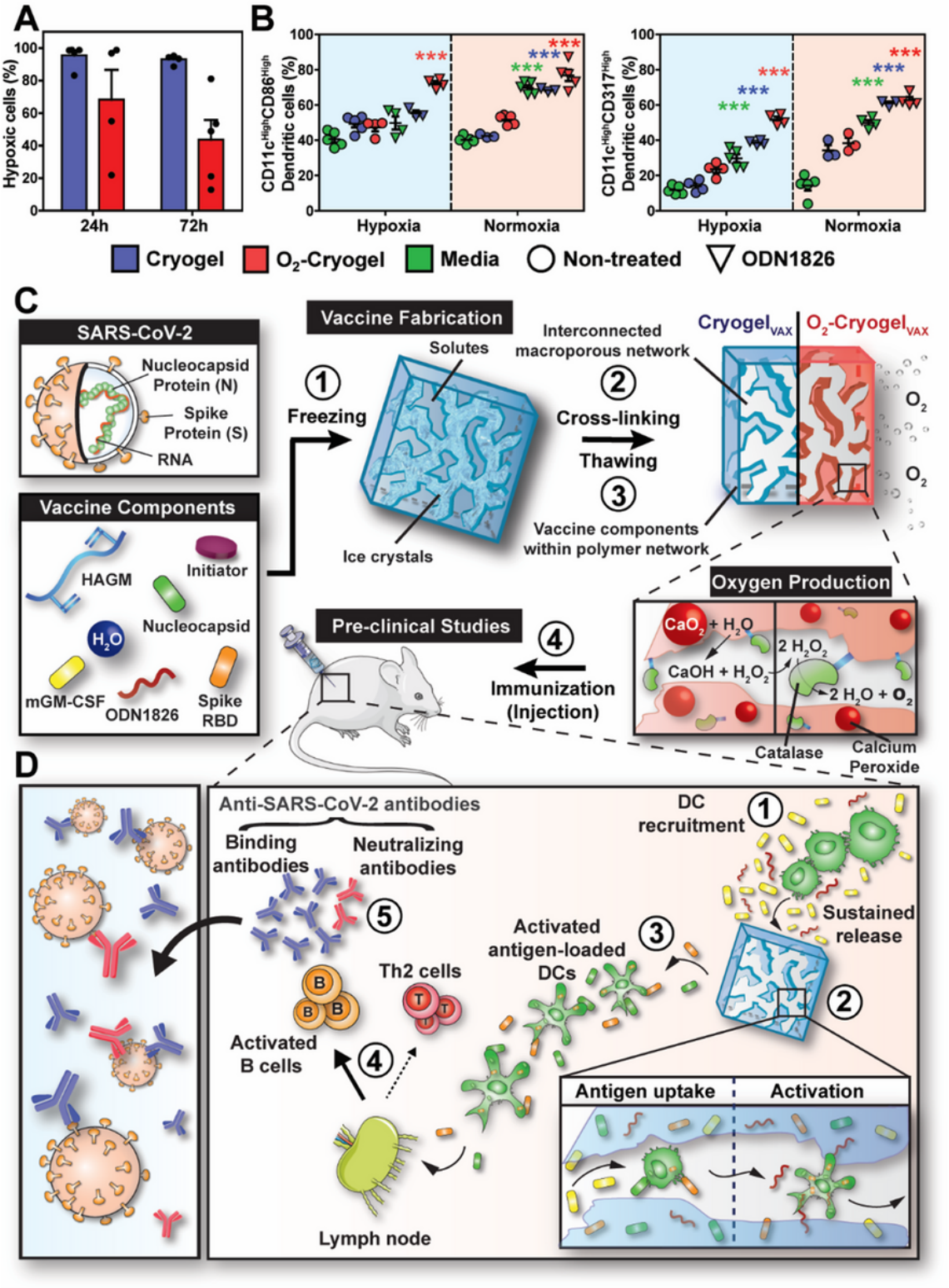

Figure 1

Cryogel-based vaccines reinforce DC-mediated immune responses. (A) Quantification of cellular hypoxia in cells recruited within Cryogels and O2-Cryogels 24 h and 72 h post-subcutaneous injection in mice. (B) Quantitative flow cytometric measurements of CD86High and CD317High dendritic cells (CD11cHigh) in Cryogels or O2-Cryogels in presence or absence of CpG-ODN 1826 in hypoxia and normoxia for 24 h (right panel). Values represent the mean ± standard error of the mean (SEM, n=5 per group). ***P < 0.001. (C)

Overview of the process for fabrication and evaluation of cubiform cryogel and O2-Cryogel vaccines. Step 1 involves freezing vaccine components, enabling crosslinking of solutes around ice crystals (step 2). Thawing results in an interconnected macroporous network with vaccine components encapsulated within the polymer network (step 3). Addition of calcium peroxide and catalase to the vaccine components before cryogelation produces O2-CryogelVAX capable of sustained production of oxygen. In step 4, cryogels are subcutaneously injected into mice for preclinical vaccine studies. (D) Illustration describing a model for DC-mediated cryogel-induced immunity. HAGM: hyaluronic acid glycidyl methacrylate; initiator: ammonium persulfate and tetramethylethylenediamine.

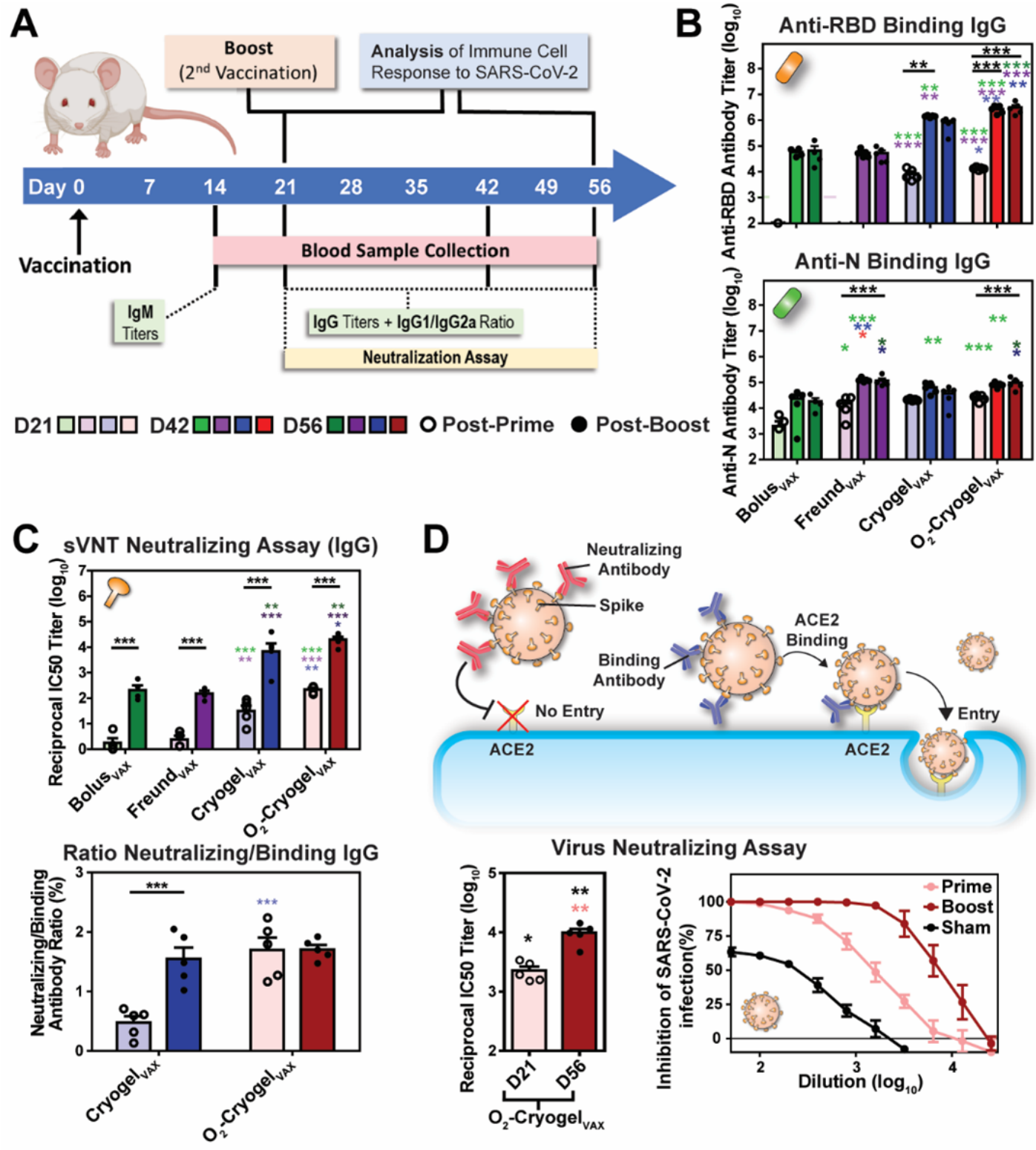

Figure 2

O2-CryogelVAX induces robust binding and neutralizing antibody responses against SARS-CoV-2 in mice. (A) Study timeline describing the vaccination regimen (BALB/c mice; n=5 per group) and the timing of the different sample collection and immuno-assay performed in this study. (B) Endpoint titers of RBD- and N-specific IgG antibody determined by ELISA at day 21, 42, and 56. (C) SARS-CoV-2 surrogate virus neutralization test (sVNT) and binding/neutralizing antibody ratio at day 21 and 56. (D) Neutralization

assay using VeroE6 cells infected with authentic SARS-CoV-2. Neutralizing antibodies from O2-CryogelVAX-treated mice were tested after prime (day 21: D21) and prime-boost (day 56: D56) immunizations. Data points show individual serum sample, and data is represented as mean ± SEM. *P < 0.05, **P < 0.01 and ***P < 0.001.

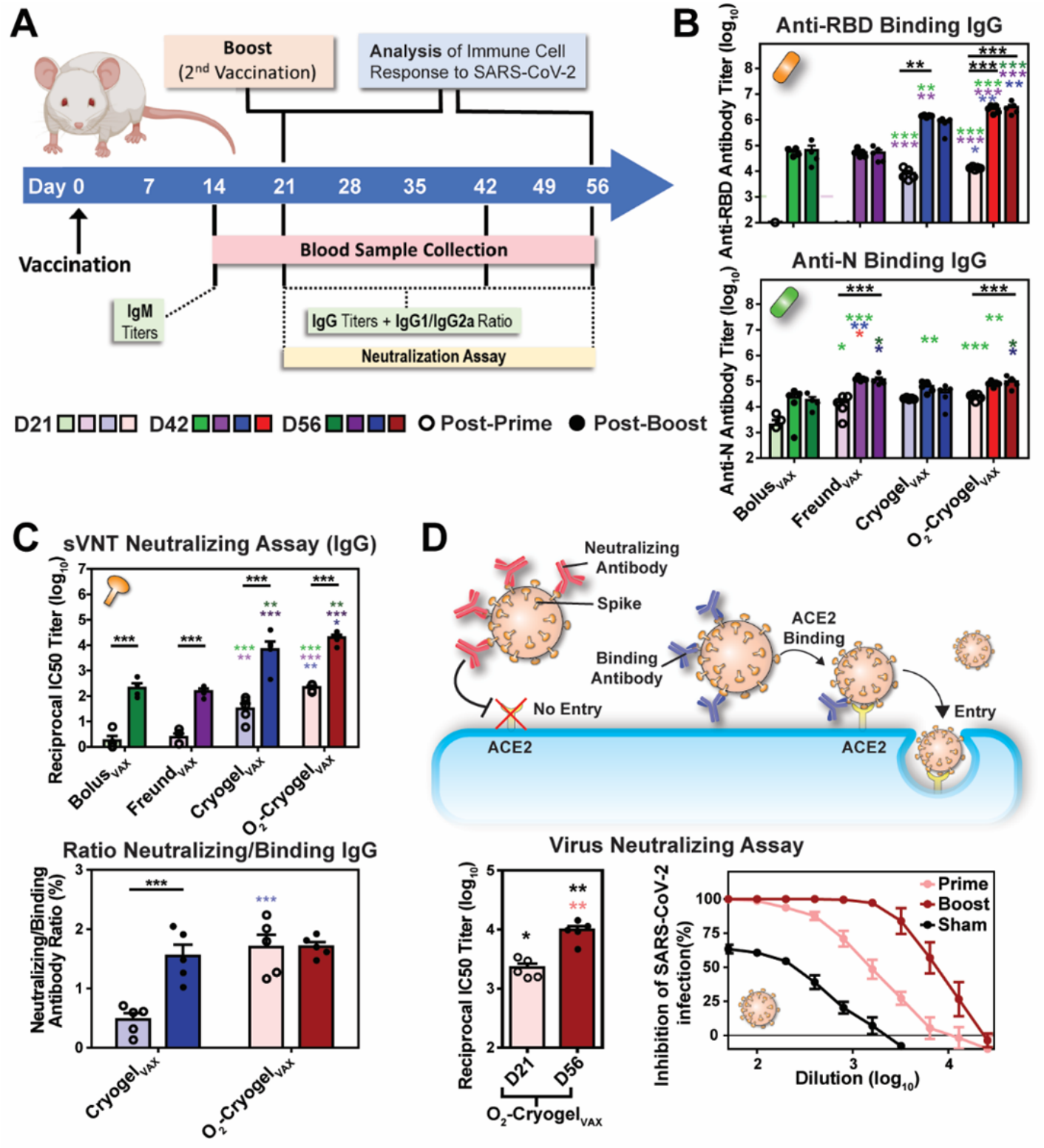

Figure 2

O2-CryogelVAX induces robust binding and neutralizing antibody responses against SARS-CoV-2 in mice. (A) Study timeline describing the vaccination regimen (BALB/c mice; n=5 per group) and the timing of the different sample collection and immuno-assay performed in this study. (B) Endpoint titers of RBD- and N-specific IgG antibody determined by ELISA at day 21, 42, and 56. (C) SARS-CoV-2 surrogate virus neutralization test (sVNT) and binding/neutralizing antibody ratio at day 21 and 56. (D) Neutralization assay using VeroE6 cells infected with authentic SARS-CoV-2. Neutralizing antibodies from O2-CryogelVAX-treated mice were tested after prime (day 21: D21) and prime-boost (day 56: D56) immunizations. Data points show individual serum sample, and data is represented as mean ± SEM. *P < 0.05, **P < 0.01 and ***P < 0.001.

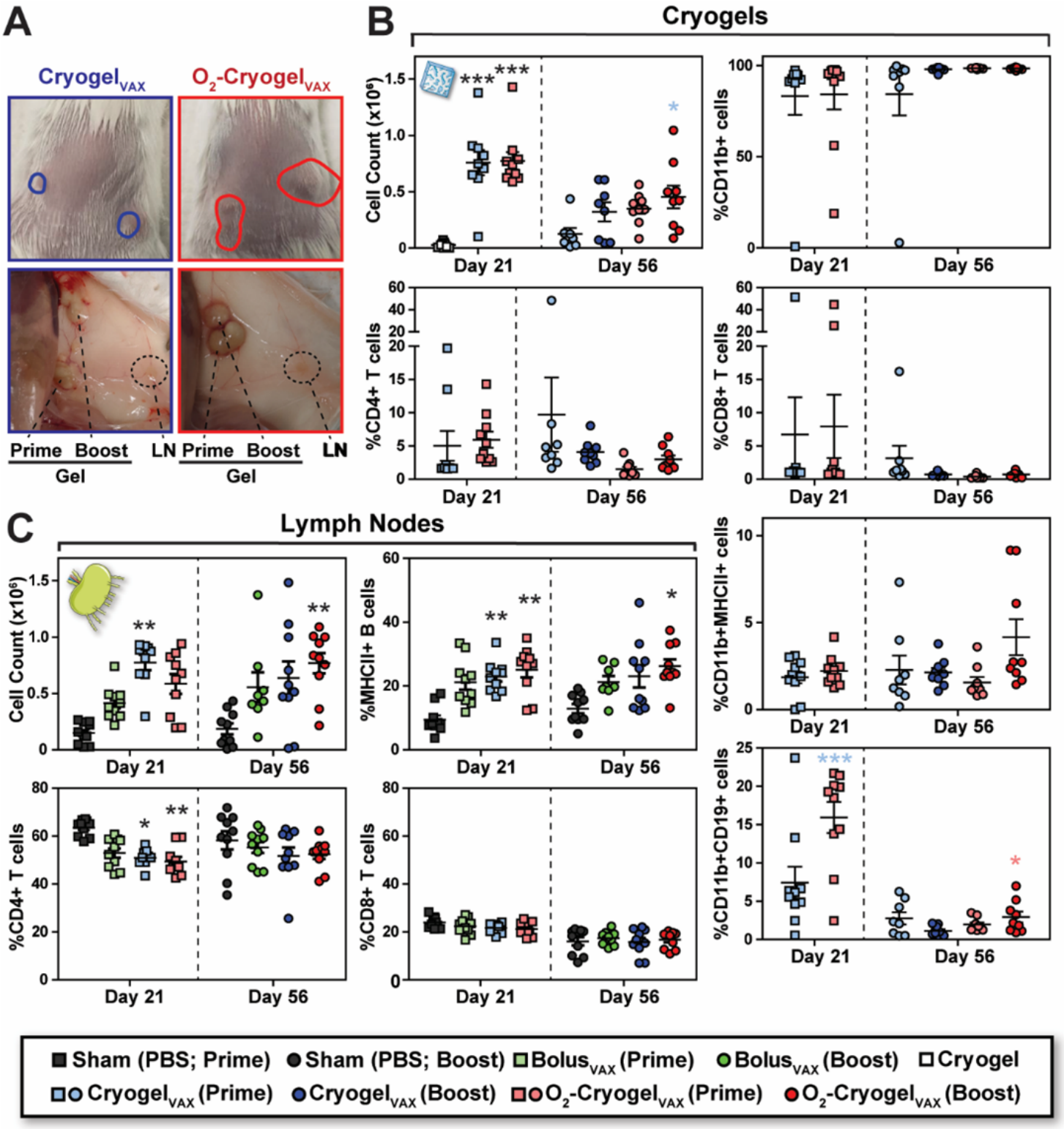

Figure 3

O2-CryogelVAX recruits high number of CD19+ leukocytes and stimulates the production of B cells in LNs. (A) Photographs of cryogels and LNs at day 56 after subcutaneous injection. (B-C) Immune cell populations in cryogels (B) and LNs (C) as analyzed by flow cytometry. Two draining LNs and cryogels were analyzed per animal. Data points show individual LNs or cryogels, and data are represented as mean ± SEM (n=10). *P < 0.05, **P < 0.01 and ***P < 0.001.

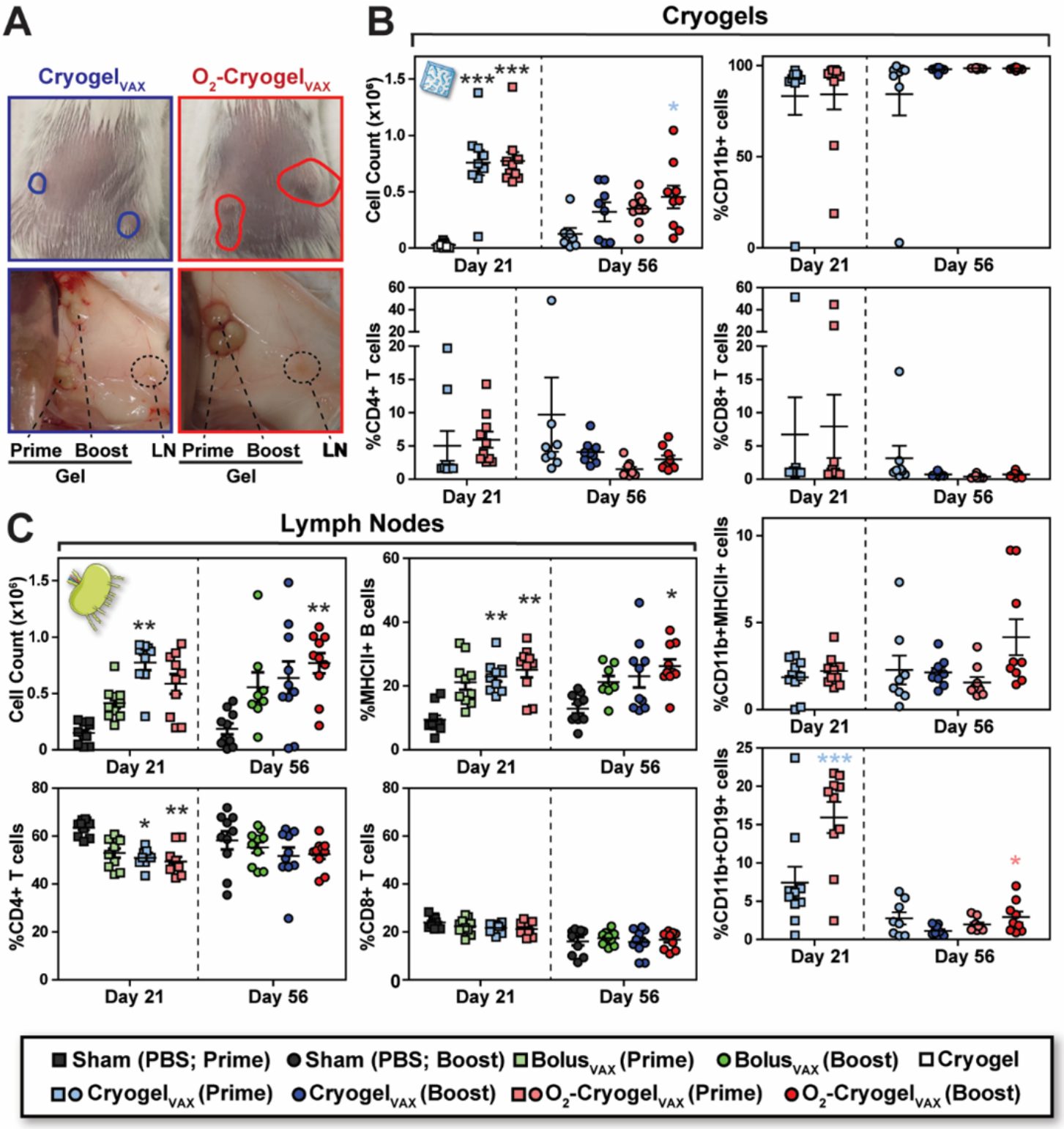

Figure 3

O2-CryogelVAX recruits high number of CD19+ leukocytes and stimulates the production of B cells in LNs. (A) Photographs of cryogels and LNs at day 56 after subcutaneous injection. (B-C) Immune cell populations in cryogels (B) and LNs (C) as analyzed by flow cytometry. Two draining LNs and cryogels were analyzed per animal. Data points show individual LNs or cryogels, and data are represented as mean ± SEM (n=10). *P < 0.05, **P < 0.01 and ***P < 0.001.

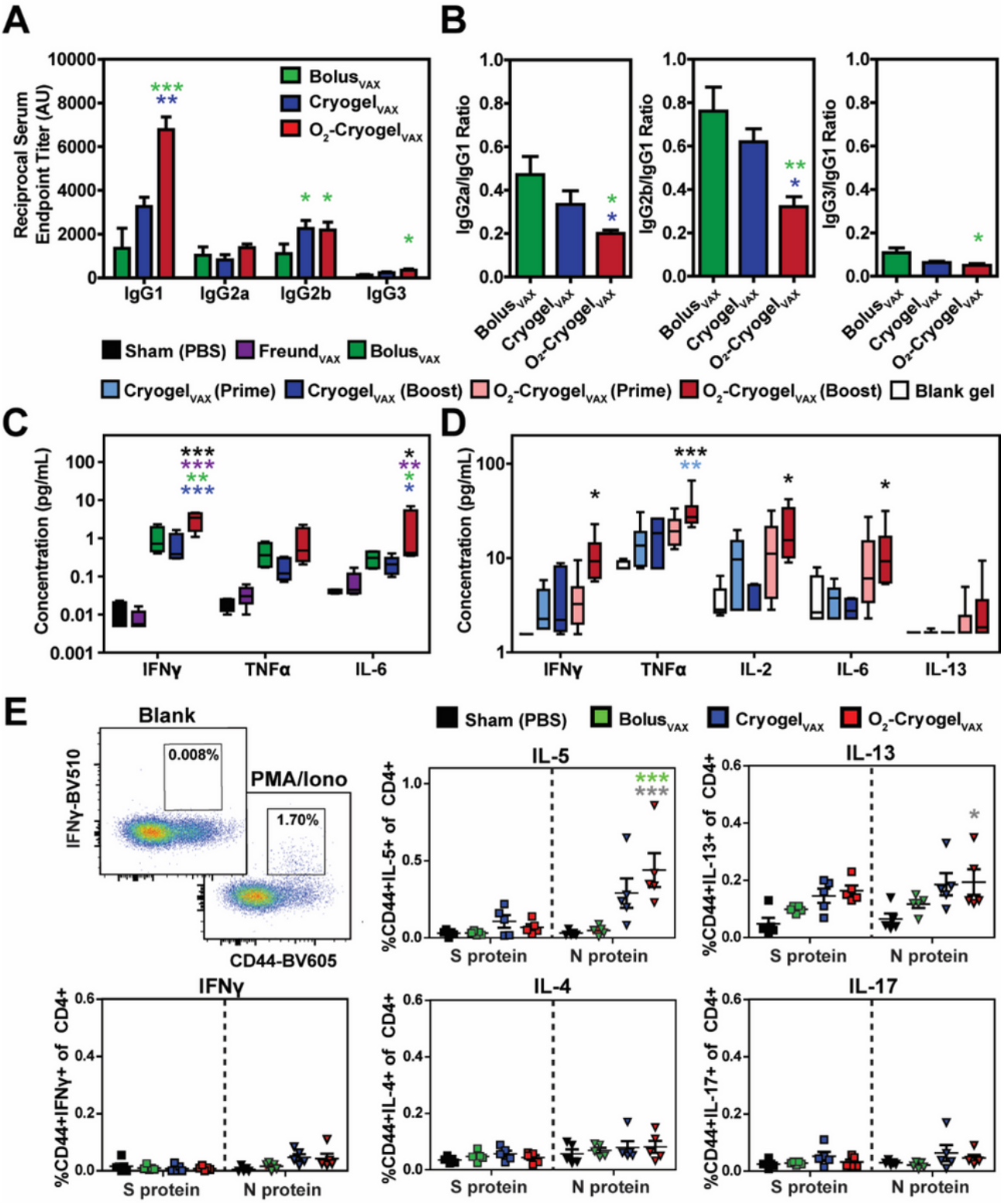

Figure 4

Immunization with O2-CryogelVAX triggers a balanced Th1/Th2-mediated immune response against SARS-CoV-2. (A) Endpoint titers and (B) endpoint titer ratios of the different IgG subclasses after 56 days were assessed by ELISA. Th1 and Th2 cytokine levels were measured in mouse serum at day 24 (C) and in explanted cryogels at day 56 (D) by multiplex assay. (E) Gating and frequencies of cytokine-producing CD44-positive CD4+ T cells after S and N protein-derived peptide stimulation of splenocytes isolated at

day 21, as quantified by flow cytometry. Data are represented as mean ± SEM (n=5) (A-D) or values of individual spleens (E). *P < 0.05, **P < 0.01 and ***P < 0.001.

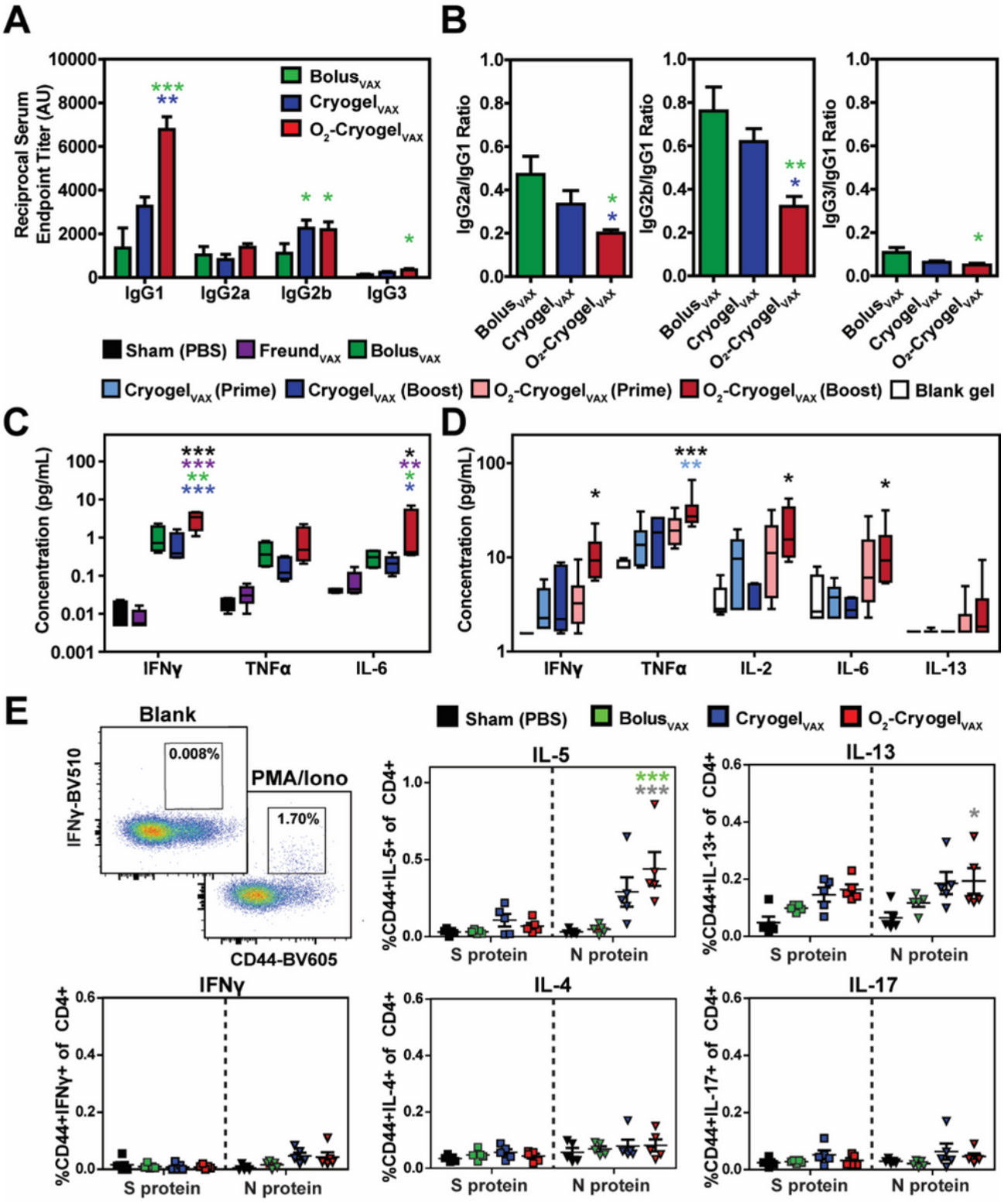

Figure 4

Immunization with O2-CryogelVAX triggers a balanced Th1/Th2-mediated immune response against SARS-CoV-2. (A) Endpoint titers and (B) endpoint titer ratios of the different IgG subclasses after 56 days were assessed by ELISA. Th1 and Th2 cytokine levels were measured in mouse serum at day 24 (C) and

in explanted cryogels at day 56 (D) by multiplex assay. (E) Gating and frequencies of cytokine-producing CD44-positive CD4+ T cells after S and N protein-derived peptide stimulation of splenocytes isolated at day 21, as quantified by flow cytometry. Data are represented as mean ± SEM (n=5) (A-D) or values of individual spleens (E). *P < 0.05, **P < 0.01 and ***P < 0.001.

Supplementary Files

This is a list of supplementary files associated with this preprint. Click to download.

- SupplementaryInformation.docx
- SupplementaryInformation.docx